Effect of Rotational Cone on Penetration Resistance and Its Implication to the Design of a Bio-Inspired Self-Burrowing Robots

Yong Tang, S.M.ASCE¹; and Junliang (Julian) Tao, Ph.D., A.M.ASCE²

¹School of Sustainable Engineering and the Built Environment, Arizona State Univ., Tempe.

Email: ytang116@asu.edu

²School of Sustainable Engineering and the Built Environment, Arizona State Univ., Tempe.

Email: julian.tao@asu.edu

ABSTRACT

A previous study by the authors showed that the rotational movement of a penetrating rod could reduce the penetration resistance. In this study, the effect of rotation on penetration is further studied to shed light on the design of a seed-inspired self-burrowing robot. Three penetration strategies were modeled using the discrete element method: (1) control case, (2) whole-body-rotation (WBR) case, and (3) cone-rotation (CR) case. It was observed that the cone penetration resistance could be reduced to similar levels due to WBR and CR at the same rotational speed. Further analysis of particle—penetrator contact data unveils that rotation of the cone reduces the contact number, and the magnitude of the contact forces. A slight reduction of the shaft friction is also observed in WBR cases, yet with a cost of much higher energy consumption to induce the rotation of the shaft. Comparing the three penetration strategies, the CR strategy is considered the most suitable for a self-burrowing robot as it reduces penetration resistance with the lowest energy consumption.

Keywords: rotation, reduction, energy consumption, particle-probe contacts

INTRODUCTION

Self-burrowing robots are a new class of robots which move themselves in soil and can be used for a spectrum of applications such as autonomous and active site investigation, precision agriculture, subsurface monitoring, and construction (Tao and Huang 2021). To be able to move in soil, the robot needs to overcome the resistance from soil, which can be orders of magnitude higher than that from air or water. Recently, several self-burrowing robots have been reported (Sadeghi et al. 2014; Winter et al. 2014; Naclerio et al. 2018; Huang et al. 2020; Okwae 2020; Tao et al. 2020; Li et al. 2021). Penetration resistance reduction strategies such as fluidization (Naclerio et al. 2018) and expansion (Tao et al. 2020) have been implemented in the design of self-burrowing robots.

Another way to reduce the resistance is rotation. Stamp (1984) found that the seed of *Erodium cicutarium* can bury itself into the ground by repeating the uncoiling-recoiling movements of the awn, triggered by periodic humidity changes. The periodical coiling-uncoiling motions lead to a rotational penetration movement of the seed, which facilitates the self-burial process for future germination.

Jung et al. (2014; 2017) observed the self-burial process of the seeds of *Erodium* and *Pelargonium* species and concluded that the rotation greatly reduces the penetration resistance. The experiments were conducted with a conical intruder of 0.2 mm/s penetrating into the glass

beads. Meanwhile, the glass beads container rotates with different rotational velocities. They assumed that the rotation of the intruder yields additional intergranular motions, which leads to the breaking of the force chain networks, thereby reducing the vertical drag forces. Besides, a mathematical model was developed to empirically correlate the drag force with the relative slip velocity of the grains (the ratio between the tangential velocity and the vertical velocity). Using DEM, Tang and Tao (2021) showed that the whole-body rotation of a cone penetrator can significantly reduce the total penetration resistance and the reduction mainly comes from the cone. Based on the results, it is hypothesized that rotation of the shaft does not reduce the cone penetration resistance, and rotation of the cone alone results in a comparable reduction in penetration resistance comparing with whole-body rotation. This study tests this hypothesis using DEM, compares the energy consumption involved in different penetration strategies, and discusses implications to the design of self-burrowing robots.

METHODOLOGY

Since this is a follow-up study to Tang and Tao (2021), the general introduction on the DEM method and the justification for selecting model parameters are not duplicated here. Only the key model parameters are provided for completeness. Moment Transfer Law (MTL) (Belheine, N. et al. 2009) was introduced to account for the effects of sand particles' roughness and irregularity in this study.

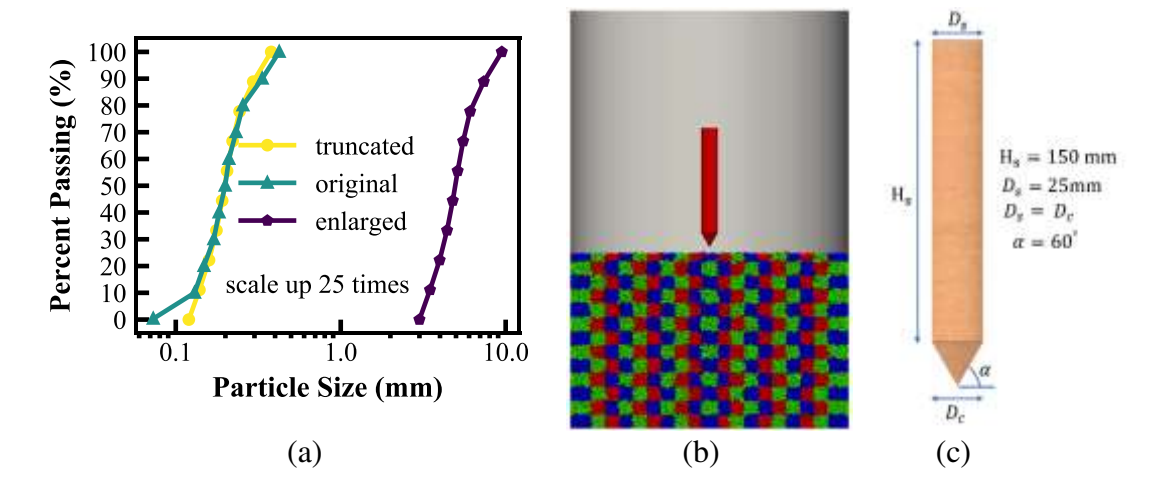


Figure 1. Simulation setups: (a) Particle size distribution; (b) penetration test sample; (c) penetrator model

Model Construction. A virtual calibration chamber is constructed with geometrical considerations to reduce the boundary effect (Arroyo et al. 2011) (cone-to-particle diameter ratio, n_p , chamber-to-cone diameter ratio, R_d , and sample height-to-cone diameter ratio, n_h). The geometric ratios are 5, 16, and 10 for n_p , R_d , and n_h , respectively (Figures 1b and 1c). Ottawa sand F65 was modeled but with a modified particle size distribution: small particles were neglected, and particle sizes were then scaled up by 25 times (Figure 1a). Butlanska (2014) found that there is no significant effect on the macroscale properties of the sand if the particle size is scaled up by 50 times in DEM. The calibrated parameters for dry Ottawa sand F65 are shown in Table 1. A loose sample of a target porosity of 0.412 is generated using a "pluviation"

method. The detailed information of the dimensions of the penetrator is shown in Figure 1c. Both the shaft and cone consist of 30 segments. The penetrator locates at 0.01 m right above the top surface of the sample at the beginning (Figure 1b).

Three penetration cases were conducted with a common vertical velocity (0.04 m/s). In the control case, the cone penetrator was pushed into the soil sample directly without rotation. In the whole-body-rotation (WBR) case, both the cone and the shaft of the penetrator were rotated at 100 rpm during penetration, and in the cone-rotation (CR) case, only the cone was rotated at 100 rpm during penetration. It should be acknowledged that the WBR and CR are different rotational mechanisms, and more systematic investigation on different combinations of vertical velocity and rotational velocity should be conducted. As a preliminary study, this paper concerns only on the differences between WBR and CR, so only one set of vertical and rotational velocities is considered in this study.

Parameters	Values	
Sample Size (mm)	400*400*250	
Number of Particles	367000	
Interparticle Friction Angle (°)	19.5	
Normal Stiffness (MPa)	400	
Density (kg/m ³)	2648	
Stiffness Ratio (α)	0.3	
Porosity (ρ)	0.412	
Rolling (Bending) Strength (η)	0.5	
Rolling Stiffness Coefficient (B)	0.2	

Table 1. Microscale Parameters for Ottawa Sand F65

Data Analysis. The general form of the total vertical resistive force (F_{z_cone} , also known as the cone resistive force) experienced by a cone can be expressed as the sum of the vertical component of contact normal forces ($F_{zn-cone}$) and that of the contact shear forces ($F_{zt-cone}$), as shown in Eq. 1.

$$F_{z-cone} = F_{zn-cone} + F_{zt-cone} = \sum_{i=0}^{n} F_{zni} + \sum_{i=0}^{n} F_{zti}$$
 (1)

The equation indicates that the cone resistive force (F_{z_cone}) is related to the number of particles that contact the cone (n), as well as the vertical component of the contact normal force (F_{zni}) and that of the contact shear force (F_{zti}) for each contact particle. In the following section, each component will be investigated subsequently to shed light on the mechanism of the reduction of cone resistive force due to the rotational movement.

Resistive torques (T) on the cone and shaft are generated when particles resist the rotational movement of the penetrator. It is necessary to calculate the resistive torque and overall energy consumed by the translational and rotational movement, as they are important for the design of a robot. The overall energy consumption (W) can be expressed as the sum of the energy consumed by the translational movement (W_{trans}) and by the rotational movement (W_{rot}) , as shown in Eq. 2. Since there is no translational movement in the xy plane and rotational only occurs around the z axis, the overall energy consumption can be simplified as Eq. 3.

$$W = W_{trans} + W_{rot} = F * s + T * \theta \tag{2}$$

$$W = F_z * s + T_z * \theta = (F_{z-cone} + F_{z-shaft}) * s + (T_{z-cone} + T_{z-shaft}) * \theta$$
 (3)

The penetrator's total vertical resistive force and torque were denoted as F, and T. s and θ are the penetration depth (m) and rotational angle (°). $F_{z\text{-}cone}$, $T_{z\text{-}cone}$, $F_{z\text{-}shaft}$, and $T_{z\text{-}shaft}$ are the vertical components of the forces and torques on the cone and shaft. All components (s, θ , $F_{z\text{-}cone}$, $T_{z\text{-}cone}$, $T_{z\text{-}shaft}$) can be measured from DEM along the penetration process.

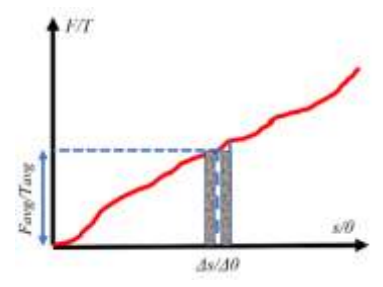


Figure 2. Schematic diagram of the energy consumption calculation

The total resistive force and torque (F, T) varies with the penetration depth. The calculation method for energy consumption is illustrated in Figure 2. The penetration depth/rotation angle and resistive force/torque were recorded every 1000 timesteps (one interval). The resistive force/torque (F_{avg}/T_{avg}) for each interval was obtained by averaging the resistive force/torque between any two neighboring intervals. Energy consumption for each interval was estimated by multiplying the average resistive force/torque by the corresponding penetration depth/rotation angle of that interval $(\Delta s/\Delta\theta)$. The overall energy consumption was estimated by summing the energy from all the intervals.

RESULTS AND DISCUSSIONS

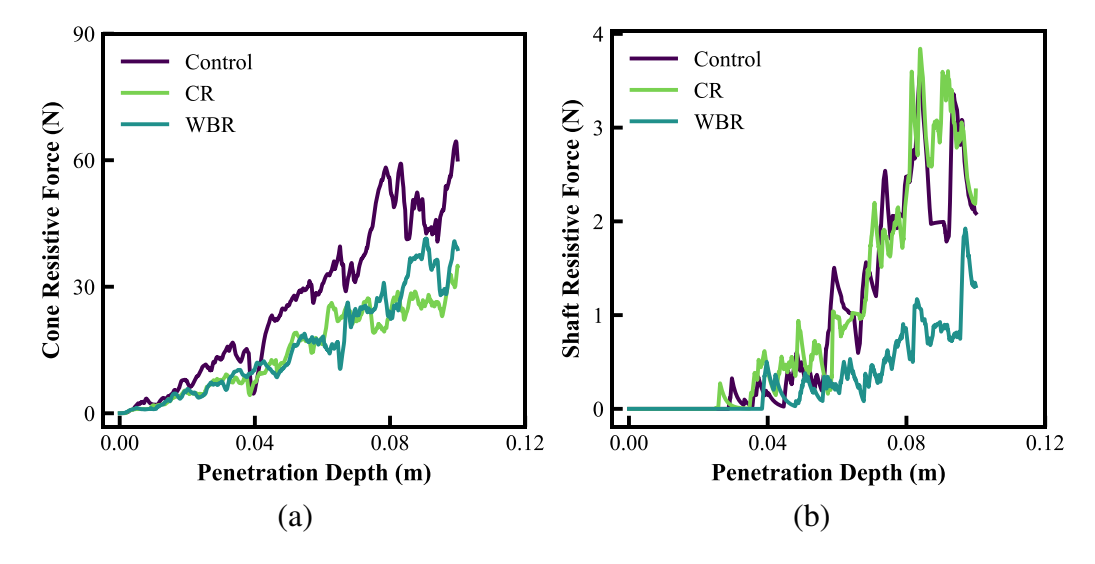


Figure 3. Resistive force for different cases: (a) cone; (b) shaft

Resistive Forces. The resistive forces (F_z -cone, F_z -shaft) for different cases are shown in Figure 3. The cone resistive forces for the rotational cases (WBR, CR) are comparable and lower than that of the control case at the same penetration depth, as shown in Figure 3a. This implies that the reduction of cone resistance is caused by the rotation of the cone, and shaft rotation does not contribute to further reduce the total resistance on the cone. The shaft resistive forces for the CR case and the control case are comparable and higher than that of the WBR case (Figure 3b). Although the rotation of the shaft reduces the shaft resistive force, the magnitude of the shaft resistive force is significantly smaller than that of the cone resistive force for each case.

Force Components. The cone resistive force components (F_{zn} -cone and F_{zt} -cone) for each case during the penetration process are shown in Figure 4. Both the F_{zn} -cone and F_{zt} -cone increase with the increasing penetration depth. The F_{zn} -cone and F_{zt} -cone for the control case are larger than those for the WBR case and CR case. F_{zn} -cone and F_{zt} -cone are nearly the same between the WBR case and the CR case. However, F_{zn} -cone contributes more to the cone resistive force than F_{zt} -cone.

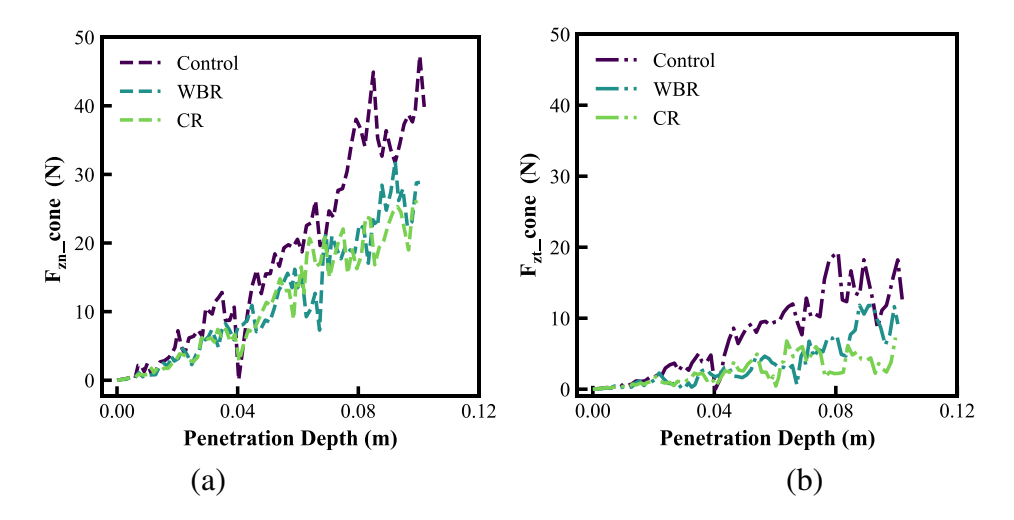


Figure 4. Cone resistive force components for different cases: (a) the vertical component of the contact normal force $(F_{zn}\text{-}cone)$; (b) the vertical component of the contact shear force $(F_{zr}\text{-}cone)$

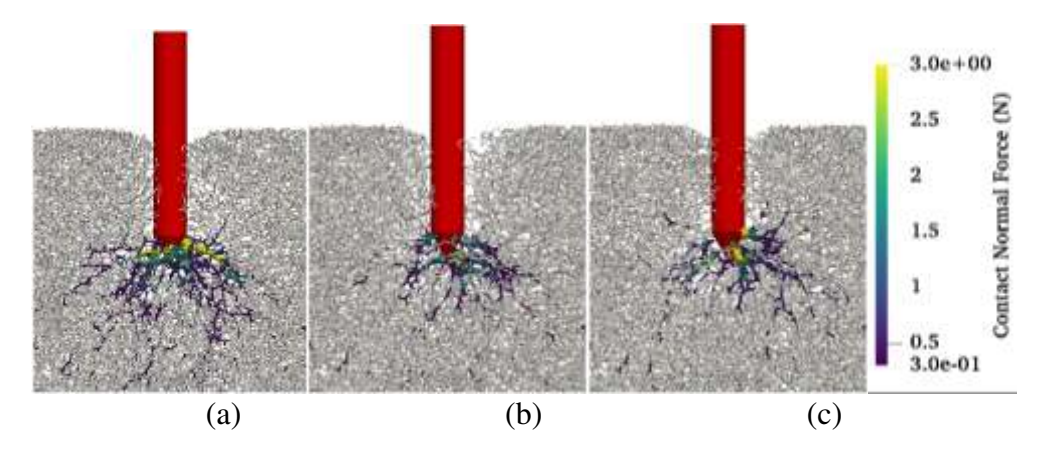


Figure 5. Force chain network under different cases at the final stage: (a) control case; (b) WBR case; (c) CR case (penetration depth = 0.10 m)

Force Chain. Figure 5 visualizes the force chain networks for different cases at the penetration depth of 0.10 m. The strong force chains locate around the cone, and the strong force chains of the rotational cases (WBR, CR) become weaker and sparser when compared to that of the control case. Besides, the contact number on the shaft for the WBR case is smaller than that for the control and CR case. It implies that the rotation of the shaft will further disturb the soil sample.

Contact Number. The contact number on the cone and shaft for different cases are shown in Figure 6. The cone contact number increases with the increasing penetration depth before the cone is fully submerged. After that, the cone contact number reaches a contact value with certain fluctuations, as shown in Figure 6a. The dashed line indicates the average cone contact number after the cone is fully submerged into the sample. The cone contact numbers are 42, 39, and 36 for the control case, WBR case, and CR case, respectively. The shaft contact number increases with the increasing penetration depth, while the shaft contact number for the control case is nearly the same as that for the CR case. The shaft contact number for the WBR case is smaller than that for the other two cases. The variations of the cone contact number might be due to the segment numbers of the cone and the relative density of the soil sample. Both the shaft and cone consist of 30 segments. There might be more than one contact between the spheres and the edges/vertices of the cone/shaft. Besides, the loose condition of the soil sample makes the conesphere contact number change very easily.

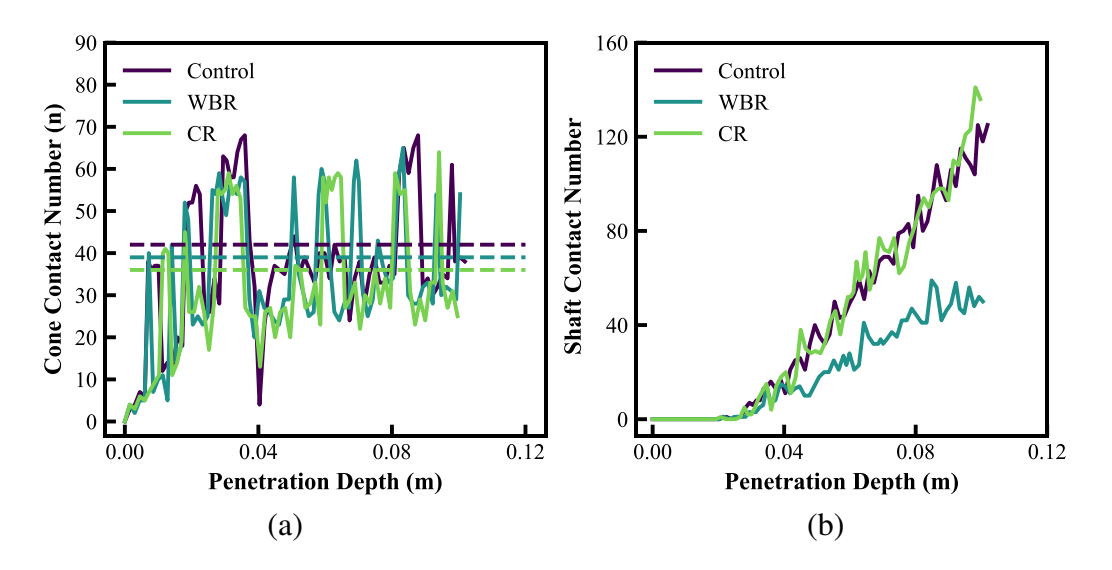


Figure 6. Contact number for different cases: (a) cone; (b) shaft

IMPLICATIONS TO THE DESIGN OF SELF-BURROWING ROBOT

The above analysis indicates that the penetration resistance reduces to a similar level for both WBR and CR cases. Lower penetration resistance is beneficial for self-burrowing robots. However, force requirement is not always the only design consideration. Power, which lumps the effects from force/torque and speed, is an important design parameter. Since rotation consumes energy, it is necessary to compare the power of each case.

Torque. The resistive torques on the cone and shaft for different cases are shown in Figure 7. Ideally, there should be no resistive torque for the control case since the cone did not rotate

during the penetration process. However, there is a net torque in the control case during the penetration process (Figure 7a). A plausible reason is that the sample is not homogeneous; the contact forces on the cone are not symmetrical, and the resultant force is off from the axis of symmetry of the cone. This torque is in the counterclockwise direction (or positive z-direction). When the cone rotates in the counterclockwise direction in the WBR and CR cases, the resistive torque on the cone changes to clockwise (or negative z-direction), and the magnitudes for the two cases are comparable and increases with depth (Figure 7a). The shaft resistive torque for the control case and CR cases is near zero during the penetration process, whereas that for the WBR case increases with depth. The maximum total torque is around 0.08 N.·m with the penetration depth at 0.10 m. This value is slightly smaller than that (0.1 N·m) for a penetrator with the same dimension and shape penetrating into the 3-mm glass beads in our recent experiment results. What's more, our recent experiment also shows that the resistive torque decreases with the increase of the angularity of the soil particles under the same vertical and rotational velocities. Therefore, the simulated results are considered reasonable.

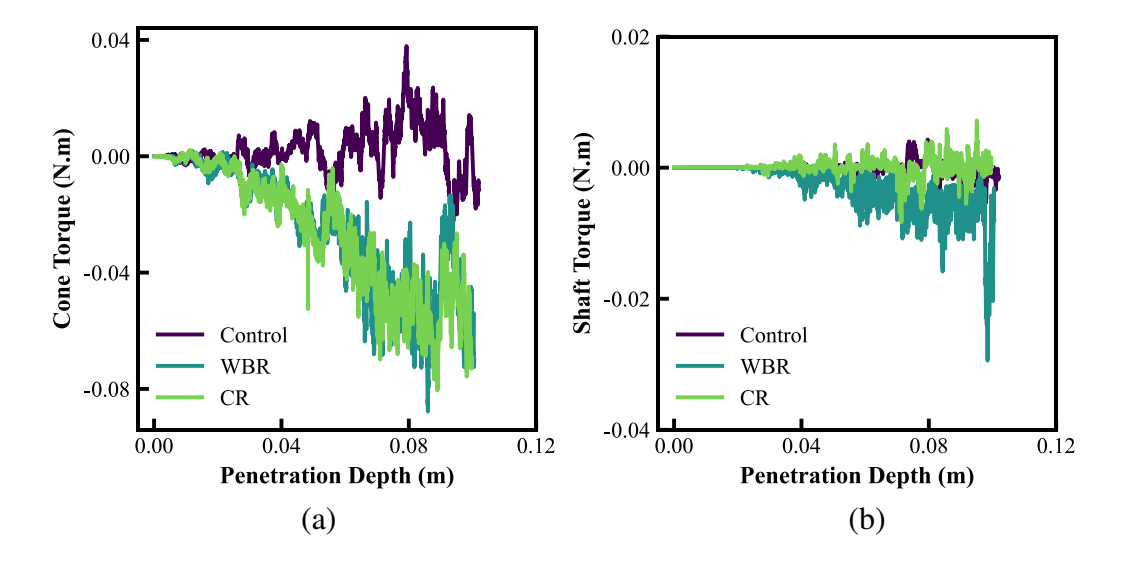


Figure 7. Torque for different cases: (a) cone torque; (b) shaft torque

Table 2. Energy consumption due to the resistive force and torque

	Control Case	WBR	CR
Force Work (J)	2.71	1.62	1.58
Torque Work (J)	0.00	0.78	0.02
Total Work (J)	2.71	2.40	1.59
Total work			
normalized by control (%)	100	88	59

Energy. Since the penetration speed is the same for all the cases, total energy instead of power is analyzed here. The total energy and its components consumed for the control case, WBR case, and CR case were shown in Table 2. The work done by the total resistive force (the sum of cone resistive force and shaft resistive force) are almost the same for the WBR (1.62 J)

and CR (1.58 J) cases, and are both considerably lower than that for the control case (2.71 J). On the other hand, the work done by the resistive torque for WBR case (0.78 J) is much larger than that for the CR case (0.02 J) and the control case (~ 0 J). This is mainly due to the energy consumed to rotate the shaft in the WBR case. The energy consumed by resistive force for the WBR, and CR cases are 60 % and 58 %, when compared with that for the control case (Figure 8). On the other hand, the energy consumed by the resistive torque for the CR case is just 2 % when comparing to that for the WBR case. Overall, the total energy consumptions for the WBR and the CR cases are 88 % and 59 %, when compared with that for the control case.

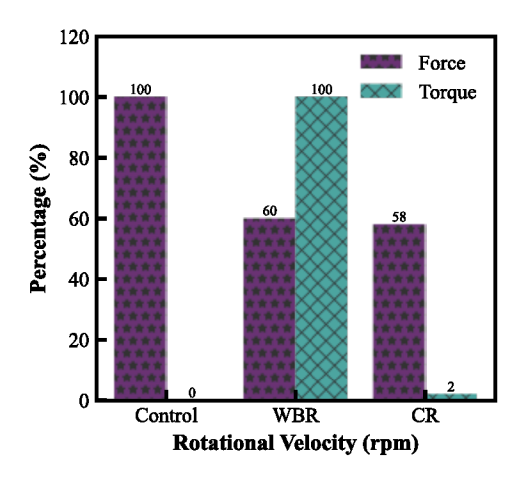


Figure 8. Energy consumption percentage through the total resistive force and torque for different cases

CONCLUSIONS

The effect of different rotational penetration strategies on penetration resistance and power is further investigated using DEM simulations in this study. The results show that the reduction of the resistive force is related to the vertical component of the contact normal force, and the contact number on the cone and shaft. It is confirmed that the cone resistive force can be reduced to a similar level for WBR and CR cases at the same rotational velocity (100 rpm). Both the vertical component of the contact normal force and that of the contact shear force are almost the same for WBR and CR cases. However, the vertical component of the contact normal force contributes more to the cone resistive force than that of the contact shear forces. The reduction of the resistive force also relates to the decrease of the contact number on the cone and shaft. The cone resistive torques were nearly the same for the WBR and CR cases, while the shaft resistive force of the WBR cases is larger as expected. The energy consumptions decrease sequentially for control cases, WBR cases, and CR cases. The CR strategy is considered the most suitable in designing a self-burrowing robot considering both force reduction and energy consumption.

ACKNOWLEDGEMENT

This material is based on the work primarily supported by the National Science Foundation (NSF) under award numbers CMMI-1841574 and CMMI-1849674. Any opinions, findings and conclusions, or recommendations expressed in this material are those of the author(s), and do not necessarily reflect those of the NSF.

REFERENCES

- Arroyo, M., Butlanska, J., Gens, A., Calvetti, F., and Jamiolkowski, M. (2011). "Cone penetration tests in a virtual calibration chamber." *Géotechnique*, 61(6), 525-531.
- Belheine, N., Plassiard, J. P., Donzé, F. V., Darve, F., and Seridi, A. (2009). Numerical simulation of drained triaxial test using 3D discrete element modeling. *Computers and Geotechnics*, 36(1-2), pp.320-331.
- Butlanska, J. (2014). *Cone penetration test in a virtual calibration chamber*.Ph.D. Thesis, Barcelona, Catalonia, Polytechnic University of Catalonia.
- Huang, S., Tang, Y., Bagheri, H., Li, D., Ardente, A., Aukes, D., Marvi, H., and Tao, J. (2020). "Effects of friction anisotropy on upward burrowing behavior of soft robots in granular materials." *Advanced Intelligent Systems*, 2(6), 1900183.
- Jung, W., Choi, S. M., Kim, W., and Kim, H.-Y. (2017). "Reduction of granular drag inspired by self-burrowing rotary seeds." *Physics of Fluids*, 29(4), 041702.
- Jung, W., Kim, W., and Kim, H.-Y. (2014). *Self-burial mechanics of hygroscopically responsive awns* Oxford University Press, 1034-1042.
- Li, D., Huang, S., Tang, Y., Marvi, H., and Aukes, D. M. (2021). "Compliant Fins for Locomotion in Granular Media." arXiv preprint arXiv:2101.03624.
- Naclerio, N. D., Hubicki, C. M., Aydin, Y. O., Goldman, D. I., and Hawkes, E. W. "Soft robotic burrowing device with tip-extension and granular fluidization." *Proc.*, 2018 IEEE/RSJ International Conference on Intelligent Robots and Systems (IROS), IEEE, 5918-5923.
- Okwae, N. K. (2020). *Design, Fabrication, and Characterization of a Sand Burrowing Robot*. Arizona State University.
- Sadeghi, A., Tonazzini, A., Popova, L., and Mazzolai, B. (2014). "A novel growing device inspired by plant root soil penetration behaviors." *PloS one*, 9(2), e90139.
- Stamp, N. E. (1984). "Self-burial behaviour of Erodium cicutarium seeds." *The Journal of Ecology*, 72(2), 611-620.
- Tang, Y., and Julian Tao, J. (2021). "Effect of Rotation on Penetration: Toward a Seed Awn-Inspired Self-Burrowing Probe." *IFCEE 2021*, 149-159.
- Tao, J. J., and Huang, S. (2021). "Burrowing Robot Breaks New Ground." *Science Robotics*, eabj3615.
- Tao, J. J., Huang, S., and Tang, Y. (2020). "SBOR: a minimalistic soft self-burrowing-out robot inspired by razor clams." *Bioinspiration & biomimetics*, 15(5), 055003.
- Winter, A., Deits, R., Dorsch, D., Slocum, A., and Hosoi, A. (2014). "Razor clam to RoboClam: burrowing drag reduction mechanisms and their robotic adaptation." *Bioinspiration & biomimetics*, 9(3), 036009.